Inline Fiber Type Identification using In-Service Brillouin Optical Time Domain Analysis

Ezra Ip¹, Yue-Kai Huang¹, Giacomo Borraccini¹, Toru Mano², Tatsuya Matsumura², Hideki Nishizawa², Andrea D'Amico¹, Vittorio Curri³, Daniel Kilper⁴, Zehao Wang⁵, Gil Zussman⁶, Tingjun Chen⁵, Koji Asahi¹ ¹NEC Labs America, Princeton, USA, ²NTT Network Innovation Labs, Yokosuka-shi, Kanagawa Japan, ³Politecnico di Torino, Torino, Italy, ¹CONNECT Centre, Trinity College Dublin, Ireland, ⁵Duke University, Durham, NC, USA, ¹Columbia University, New York, NY, USA, ¹NEC corporation, Abiko, Chiba, Japan.

Abstract: We proposed the use of BOTDA as a monitoring tool to identify fiber types present in deployed hybrid-span fiber cables, to assist in network planning, setting optimal launch powers, and selecting correct modulation formats. © 2023

1. Introduction

The achievable throughput in optical data transmission is limited by additive white Gaussian noise (AWGN) and fiber nonlinearity [1]. Prior to coherent systems, chromatic dispersion (CD) management and compensation was vital to high-speed transmission. Dispersion-shifted fiber (DSF) with its zero-dispersion wavelength inside the C-band was believed to be advantageous over standard single-mode fiber (SSMF) and was widely deployed in countries like Japan [2]. Other low-dispersion fibers such as large-effective area fiber (LEAF) are still common in legacy systems. Low-dispersion fibers suffer from increased nonlinearity penalties. In DSF, four-wave-mixing (FWM) also becomes non-negligible. Dealing with mixed fiber types can be challenging, especially if cables of different types have been spliced to create hybrid-type spans [3,4]. This may arise when a network operator has different fiber types in their inventory, and hybrid spans are created due to limited number of cables available, or due to error in cataloging and connection. This will impact optimal signal launch condition, and the system needs to be monitored and adjusted accordingly.

Commercially available coherent transponders already provide read out of accumulated CD for an optical channel, and can be used to infer fiber information [5]. However, accumulated CD alone is insufficient for determining fiber type in hybrid-fiber systems. Recently, longitudinal power monitoring (LPM) provides a method for estimating a link's nonlinearity profile, which combined with CD, can provide better detailed spatial information about fiber types [6]. However, this method requires launching the test channel at high power, and may be unsuitable for in-service monitoring. It is well known that fibers with different refractive index profiles, created using different doping profiles will exhibit different Brillouin gain spectra (BGS) [7,8]. Brillouin optical time-domain reflectometry (BOTDR) and Brillouin optical time-domain analysis (BOTDA) are two well-known methods in distributed sensing [9,10] based on measurement of BGS. In this work, we propose using BOTDA as a fiber type identification tool to assist in setting correct amplifier output powers and choosing appropriate modulation formats based on the fibers identified.

2. Experimental Setup and Results

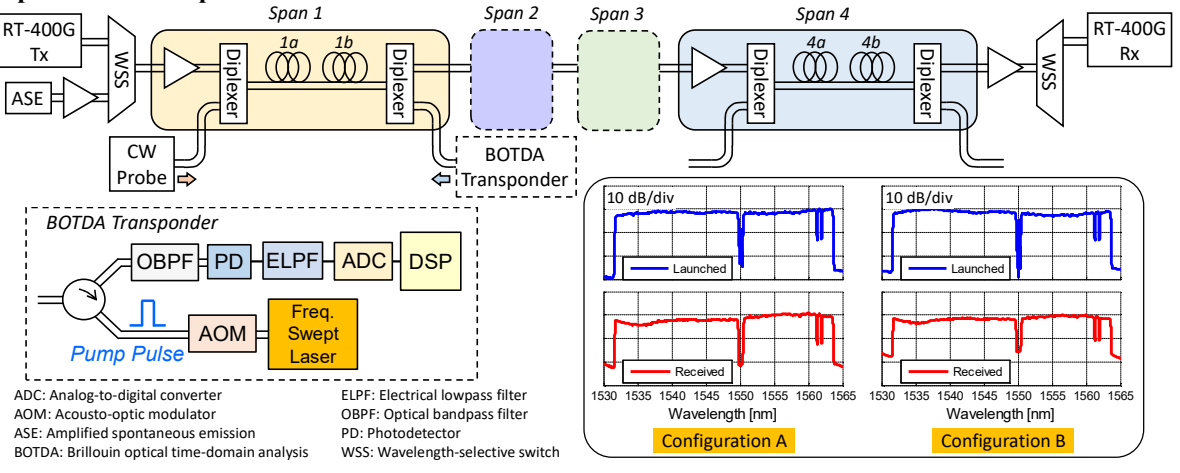


Fig. 1. Experimental setup for simultaneous data transmission and link monitoring using BOTDA for a hybrid-fiber link.

The experimental setup is shown in Fig. 1. At the transmitter, a real-time coherent CPF2 transmitter is multiplexed with noise loading and flattening using a wavelength-selective switch (WSS). The data channel is either 62.5-Gbaud 16QAM or QPSK, with net data rates of 400-Gb/s or 200-Gb/s respectively after accounting for soft-decision forward error correction (SD-FEC) and other overhead. The link comprises of four hybrid-fiber spans, with erbium-doped fiber

amplifiers (EDFA) compensating the loss of the preceding span. Two diplexers are inserted before and after the fiber span to multiplex the BOTDA channel with the emulated in-service channels. The diplexers are centered at 1550.12 nm, with 3-dB bandwidths of 100 GHz (0.8 nm). In practice, the BOTDA "monitoring" channel can be outside the spectrum used for data transmission, and inserted using the OTDR ports provided by optical line equipment.

The BOTDA transponder launches periodic pump pulses that counter-propagate against the data channels, while a continuous-wave (CW) probe signal co-propagates with the data channels. The probe power was set to -15.5 dBm. Details of the BOTDA transponder are shown in the inset of Fig. 1. The transmitter comprise of a frequency swept laser with a slew rate of 2 GHz/sec and a period of 2.5 sec driving an acousto-optic modulator (AOM) which carves pulses of 1 µs duration (100 m spatial resolution) at a repetition period of 1.25 sec, which enables interrogation up to ~130 km. After amplification, pump pulses at +23 dBm peak power are launched into the link via a circulator. At the circulator's receive port, backscatter is passed through an optical bandpass filter (OBPF) to reject both Rayleigh and Brillouin anti-Stokes components. The desired signal at the Brillouin Stokes frequency (~11 GHz below the frequency of the pump pulse) is detected by a photodetector (PD), followed by an anti-aliasing electrical bandpass filter (EBPF), followed by sampling and digitization by an analog-to-digital converter (ADC) and digital signal processing (DSP).

We performed preliminary testing of BOTDA without data transmission with only one fiber span comprising the concatenation of 25.7 km of LEAF, followed by 20 km of SSMF and 2×20.5-km spools of DSF. Fig. 2(a) shows the measured BGS maintained high fidelity even after 85 km. The BGS signatures of different fiber types can be clearly observed. We swapped the order of LEAF, DSF and SSMF as the spool closest to the BOTDA transponder and remeasured their BGS in the high SNR region. Figs. 2(b)-(d) show that SSMF has only one peak, while LEAF and DSF have multiple peaks. The peaks in LEAF are at ~189, 358 and 478 MHz, while the peaks in DSF are at ~248, 516 and 604 MHz. This contrast allows machine learning classification of fiber type based on the BGS vs distance spectrogram.

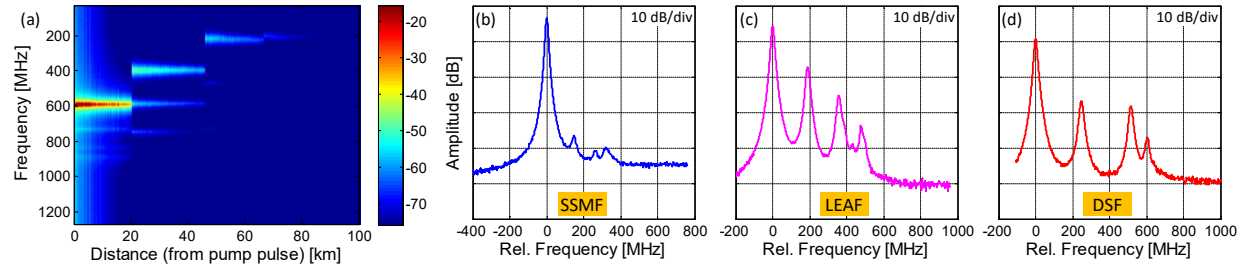


Fig. 2. BOTDA results. (a) Brillouin gain spectrum (BGS) vs distance for the concatenation of SSMF LEAF, and DSF, and BGS of (b) SSMF, (c) LEAF and (d) DSF measured at 15 km by placing these respective fibers at the front.

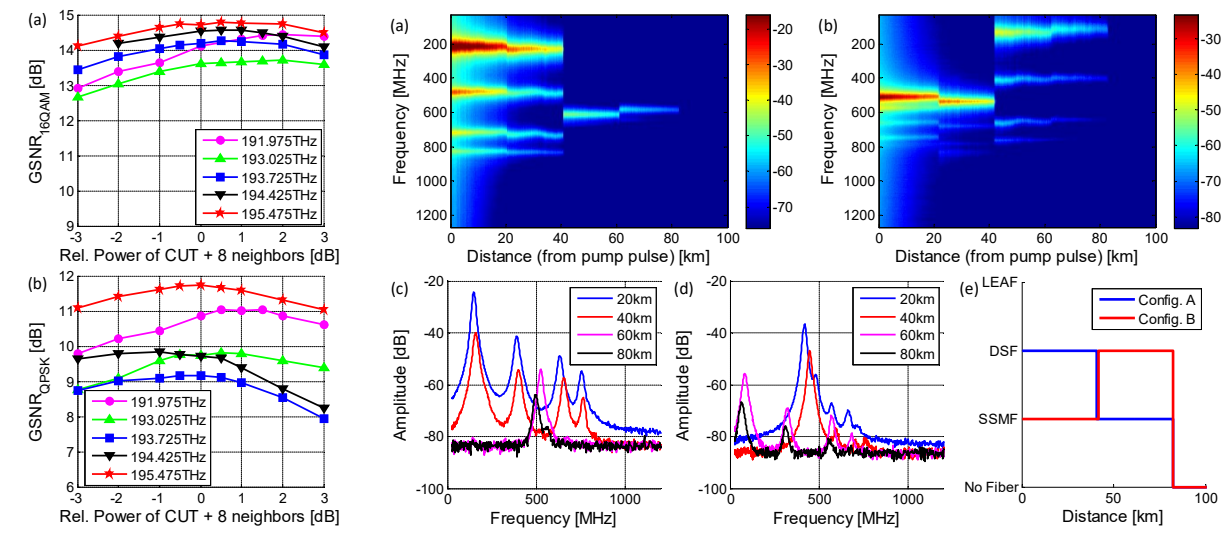


Fig. 3. BER vs launch power sweep for the CUT + 8 neighboring channels when the link is in configurations (a) A and (b) B.

Fig. 4. (a-b) BGS vs distance measured by BOTDA for Span 1 in configurations A and B, respectively, (c-d) BGS at specific distances of 20, 40, 60 and 80 km. (e) Machine learning classification of fiber types from the BGS vs distance spectrogram.

To illustrate the impact of fiber type on optimum launch power and transmission performance, we performed a biterror rate (BER) vs launch power sweep for two configurations: (A) 40 km of SSMF followed by 40 km of DSF in every span, and (B) 40 km of DSF followed by 40 km of SSMF in every span. Through numerical simulations, we estimated the optimum launch powers to be around +15 dBm and +18.6 dBm for configurations A and B, respectively. Setting the output of all EDFAs to these values, and using the transmitter's WSS to raise or lower the powers of the channel under test (CUT) and its eight nearest neighbors, Fig. 3 shows the BER sweep results for five channels at 191.975, 193.025, 193.725, 194.425 and 195.475 THz (1561.622, 1553.128, 1547.516, 1541.548 and 1533.661 nm). In config. A, the generalized SNR (GSNR) after four spans was sufficient to support 16QAM, while config. B could only support QPSK. The vertical axes in Fig. 3 shows GSNR inferred from measured pre-FEC BER, which are

 $GSNR_{QPSK} = 2 \left[erfc^{-1} \left(2 \cdot BER_{QPSK} \right) \right]^2$ and $GSNR_{16QAM} = 10 \left[erfc^{-1} \left(\frac{8}{3} BER_{16QAM} \right) \right]^2$ for QPSK and 16QAM, based on inverting theoretical BER vs SNR formulae in presence of AWGN only. In config. A, there was a slight under-estimation of optimum launch power, while in config. B, optimum launch power is lower for the channels closest to the zero-dispersion wavelength of DSF compared with channels at the edges of the C-band. These results confirm a difference of ~4 dB in optimum launch power depending on whether DSF or SSMF is immediately after the EDFA, and a reduction in constellation size is necessary when DSF is in front.

We then conducted in-service BOTDA using the spectral hole created by the diplexers in Fig. 1. As the counter-propagating pump pulse is only 1 µs (optical distance of 200 m), its impact on the data channels via Raman power transfer is negligible, even though the pulses have peak powers of +23 dBm. No impact on BER was observed regardless of whether the BOTDA system is running. The BGS vs distance spectrogram for the two configurations are shown in Figs. 4(a) and (b), while the BGS at specific distances are shown in Figs. 4(c) and (d). Note the fiber orientation seen by BOTDA is the mirror image of the link due to counter-propagation: when DSF is closest to the output of the EDFA, it is furthest from the BOTDA. Fig. 4(d) shows that multiple peaks of DSF remain visible even after 80 km. Fig. 4(e) shows the machine-learning-based fiber discriminator correctly deducing the fiber configuration.

Finally, we measured BER penalty caused by using incorrect launch power and/or modulation format. In config. A, if a launch power of +15 dBm was used assuming the link was in config. B, a slight increase in BER is observed (first two columns of Table 1), but all five channels remain error-free after FEC decoding. Config. B is far less tolerant to incorrect launch power. Launching at +19 dBm results in four of the five channels having non-zero post-FEC BER (fourth column of Table 1). Note the increase in pre-FEC BER is even worse than predicted by Fig. 3(b) since there is no walk-off effect near the zero-dispersion wavelength in DSF. Thus raising the powers of the CUT + 8 nearest neighbors does not fully account for the increase in FWM and cross-phase modulation (XPM) that would result from launching all channels at 4 dB above the optimum launch power. We considered an additional configuration C, where only Span 1 has DSF before SSMF, while Spans 2–4 have SSMF before DSF. This represents an "error" scenario where one span was incorrectly connected. In the absence of fiber identification using BOTDA, the output of all EDFAs were set to +19 dBm and the modulation format set to16QAM assuming config. A. The fifth column of Table 1 shows all five channels with BERs exceeding the FEC threshold. Using BOTDA, we confirmed that the fibers in Span 1 were switched. The output power of EDFA 1 was reduced to +15 dBm. Although 16QAM still failed due to excessive nonlinear penalty, the pre-FEC BERs using QPSK are shown in the last column of Table 1, demonstrating that inline fiber identification can be a useful diagnostic tool for network operation and maintenance.

Channel	Configuration A		Configuration B		Configuration C	
	19 dBm	15 dBm	15 dBm	19 dBm	All spans 19 dBm	First span 15 dBm, all other spans 19 dBm
	16QAM	16QAM	QPSK	QPSK	16QAM	QPSK
191.975 THz	8.5×10 ⁻³	1.8×10 ⁻²	2.1×10 ⁻⁴	(2.2×10 ⁻²)	(2.0×10 ⁻²)	1.3×10 ⁻⁶
193.025 THz	1.0×10 ⁻²	1.6×10 ⁻²	8.7×10 ⁻⁴	(2.4×10 ⁻²)	(2.2×10 ⁻²)	1.2×10 ⁻⁵
193.725 THz	9.5×10 ^{−3}	1.1×10 ⁻²	1.8×10 ⁻⁴	(2.4×10 ⁻²)	(2.2×10 ⁻²)	1.4×10 ⁻⁴
194.425 THz	6.5×10 ⁻³	8.5×10 ⁻³	9.6×10 ⁻⁴	(2.4×10 ⁻²)	(2.3×10 ⁻²)	1.8×10 ⁻⁴
195.475 THz	4.9×10 ⁻³	8.7×10 ⁻³	5.0×10 ⁻⁵	1.4×10 ⁻²	(2.3×10 ⁻²)	2.9×10 ⁻⁶

Table 1. Pre-FEC BER of five channels for different link configurations and launch powers, brackets indicate non-zero post-FEC BER.

3. Conclusions

We successfully demonstrated the use of BOTDA as a monitoring tool to identify different fiber types, their lengths, and the order they were connected in a hybrid-fiber link. Our results show that BOTDA is useful in network planning: for correctly setting amplifier output powers and selecting appropriate modulation formats for a given link.

Acknowledgments. The work was supported by NSF grants OAC-2029295, EEC-2133516, CNS-2330333, and SFI grant #13/RC/2077_P2.

4. References

- [1] P. Poggiolini, J. Lightw. Technol. 30(24), 3857-3879 (2012).
- [2] T. Croft et al, J. Lightw. Technol. 3(5), 931-934 (1985).
- [3] I. Roudas et al, Intell. and Converged Networks **2**(1), 30–49, (2021).
- [4] L. Krzczanowicz et al, OFC 2019, Paper Tu3F.4.
- [5] E. Seve et. al, ECOC 2022, Paper Mo4A.1.

- [6] M. Eto et. al, ECOC 2023, Paper Tu.A.2.3.
- [7] C. Lee et al, IEEE Photon. Technol. Lett. 13(10), 1094–1096 (2001).
- [8] F. Bastianini et al, Sensors 19(23), article 5172, (2019).
- [9] M. Niklès et al, J. Lightw. Technol. 15(10), 1842–1851 (1997).
- [10]T. Horiguchi et al, Photon. Technol. Lett. 2(5), 352-354, (1990).